

## Measurement of the $K_L^0$ - $p$ and $K_L^0$ - $d$ total cross sections\*

W. E. Cleland,<sup>†</sup> Barton Goz,<sup>†</sup> and Dietrich Freytag<sup>§</sup>

*Department of Physics and Astronomy, University of Massachusetts, Amherst, Massachusetts 01002*

Thomas J. Devlin, Robert J. Esterling,<sup>¶</sup> and Kirby G. Vosburgh<sup>¶</sup>

*Physics Department, Rutgers, The State University, New Brunswick, New Jersey 08903*

(Received 7 May 1975)

Total cross sections have been measured for the transmission of long-lived neutral  $K$  mesons through hydrogen and deuterium. The momentum range for the  $K_L^0$  was 130–550 MeV/ $c$ . The momentum of each detected kaon was measured by time of flight. The cross sections are consistent with earlier less precise results. Comparison of the  $K_L^0$  cross sections is made with the results of several  $K$ -matrix fits to other  $\bar{K}N$  data, and the  $K_L^0$  total cross sections are compared with existing theoretical calculations for  $K^-d$  total cross sections.

### I. INTRODUCTION

Using the time-of-flight method for measuring the velocity of neutral kaons at the Princeton-Pennsylvania Accelerator (PPA), we have measured the momentum dependence for the attenuation of neutral long-lived kaons by hydrogen and deuterium targets. We have thus obtained total cross sections for  $K_L^0$ - $p$  and  $K_L^0$ - $d$  scattering in the lab momentum range 130–550 MeV/ $c$ . The  $K_L^0$ - $p$  total cross sections, calculated for each 20 MeV/ $c$  momentum interval, are accurate to about 10–20%, whereas the  $K_L^0$ - $d$  total cross sections are accurate to 5–10%. An over-all normalization uncertainty, which arises from unexplained beam monitor fluctuations, amounts to 1.0 mb for data taken over the entire momentum range and 1.4 mb for data taken over a more restricted momentum range.

### II. EXPERIMENTAL DETAILS

The intensity of the long-lived kaon component of a neutral beam was measured at a point far from the production target through the detection of the  $K_L^0$  decay products. To measure the total cross section, we observed the change in this intensity as a function of momentum when a target was inserted in the beam upstream of the detector. The experiment is similar in concept and design to that of Sayer *et al.*<sup>1</sup> (referred to hereafter as I). The chief differences between that experiment and the present one are (1) the use of liquid hydrogen and deuterium targets, (2) reduction of the lower momentum cutoff of the  $K_L^0$  spectrum to 130 MeV/ $c$ , (3) increase in the kaon detector size from approximately 61 cm to 122 cm, and (4) more stringent collimation to reduce possible neutron backgrounds.

The same apparatus, with the exception of the hydrogen/deuterium target, was used in a previous

experiment by Vosburgh *et al.*<sup>2</sup> (hereafter referred to as II). The apparatus is described in detail by these authors.

#### A. Apparatus

*Beam.* The beam was produced at PPA by 3-GeV protons striking an internal platinum target 3.2 cm in length (along the beam direction), 1.3 cm high, and 0.3 cm thick. A plan view of the beam and apparatus is shown in Fig. 1. Particles emerging from the target passed through (1) a 5-cm thick lead  $\gamma$ -ray converter, (2) a sweeping magnet to remove charged particles, (3) a beam channel approximately 4.6 m long through the shield wall of the synchrotron, (4) a second sweeping magnet, (5) a primary collimator, (6) a hydrogen/deuterium target (7) a third sweeping magnet containing a secondary collimator, and (8) the kaon detector. The beam line was evacuated from the  $\gamma$ -ray converter to the downstream end of the kaon detector, except for the region where the hydrogen/deuterium target was located. The aluminum vacuum pipe in the region of the detector was 30 cm in diameter and 0.3 cm thick.

The flux of neutral kaons at the detector position was approximately 60 per second, with a kaon/neutron ratio of about  $10^{-3}$ . The proton beam spill on the synchrotron target lasted for 10 msec out of every 52 msec. Within the 10 msec burst was an rf structure which was useful for measuring the velocity of neutral particles by using a time-of-flight (TOF) technique.<sup>1,2</sup> The proton beam was divided into  $\sim 1$  nsec bunches which normally struck the target  $\sim 33$  nsec apart, but alternate bunches could be eliminated by electrostatic deflection of the proton beam at injection into the synchrotron. This gave  $\sim 67$  nsec (single-chopped) or  $\sim 134$  nsec (double chopped) separation. The useful momentum range of kaons obtained at the

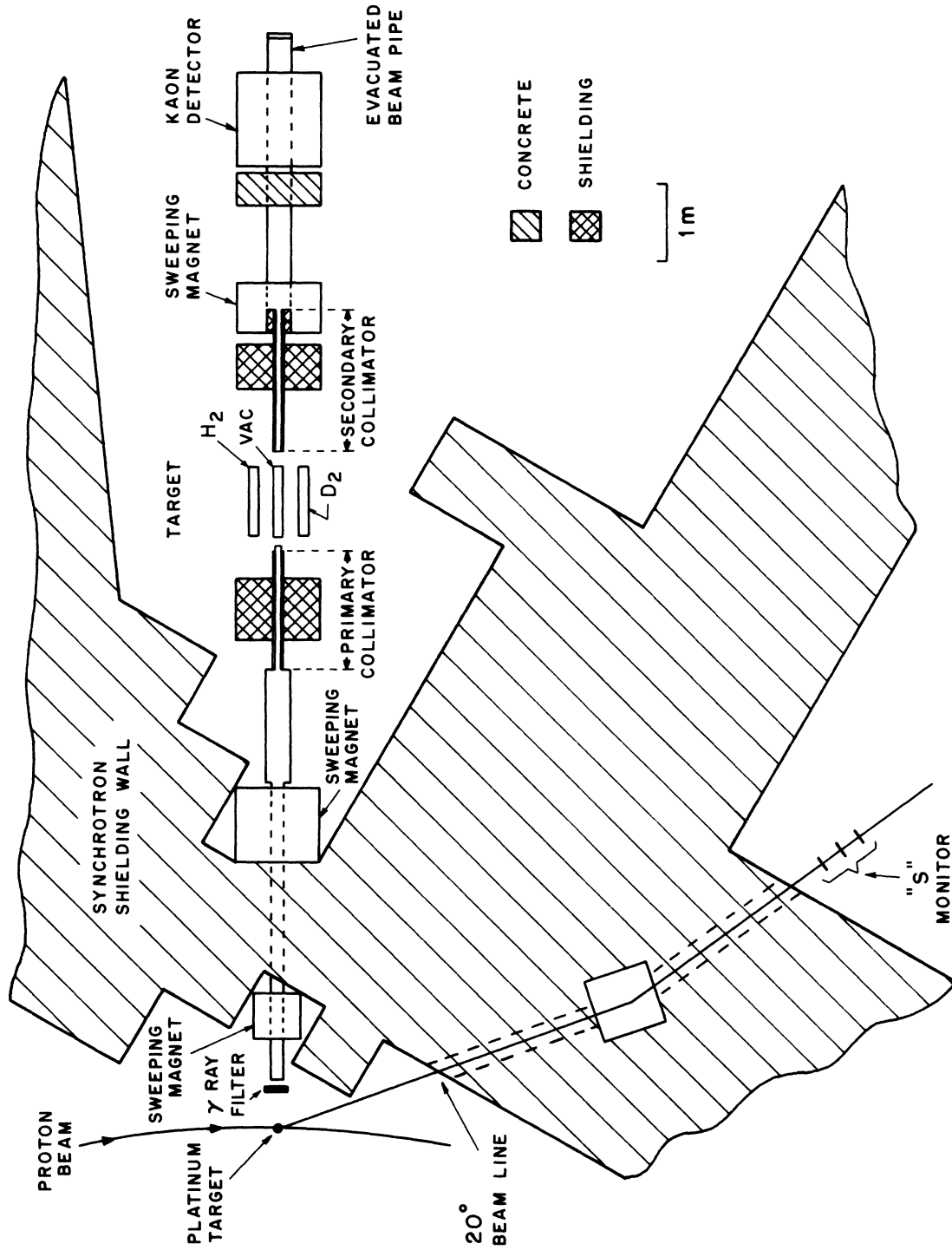


FIG. 1. Plan view of the apparatus. The neutral beam is produced by the internal synchrotron target at 90° from the proton beam. Except for the region of the hydrogen target, the entire length of the beam line is evacuated. The principal beam monitor, labeled "S," is a scintillation counter telescope placed in a momentum-analyzed beam produced at 20° from the internal target.

position of our detector extends from 130 MeV/ $c$  (double-chopped injection) or 210 MeV/ $c$  (single-chopped injection) up to 550 MeV/ $c$  with a peak in the spectrum at about 300 MeV/ $c$ . The momentum spectrum observed at the position of our detector is shown in Fig. 2.

*Collimation.* The primary (beam-defining) and secondary collimators provided a well-defined beam geometry in the regions of the target and kaon detector. The primary collimator was five feet long, with an aperture formed by a 5.7-cm diameter cylinder into which vertical shims had been inserted to leave a 4.5-cm horizontal aperture. This geometry prevented the direct beam from striking the walls of the hydrogen/deuterium target and the detector. The exit of the collimator was located 7.5 m from the synchrotron target, and the solid angle it subtended from the synchrotron target was approximately  $26 \mu\text{sr}$ . To permit measurements of background which were not related to particles in the beam, this collimator was fitted with valves at either end, so that it could be filled with mercury to stop the beam. The secondary collimator had a 5.7-cm diameter circular aperture. Its exit was located approximately 2.1 m from the center of the hydrogen target, from which point it subtended a solid angle of  $690 \mu\text{sr}$ .

An important difference between experiment I and the present experiment is that in this experiment the beam was collimated both upstream and downstream of the target. The secondary collimator prevented neutrons which scattered from the exit of the primary collimator from interacting in the detector. The authors of I ascribe a background of a few percent of their kaon rate to this effect, whereas we measured the corresponding background in our case to be less than 0.5%. We have compared the cross sections measured by using the different telescope combinations, which was the test reported in I to study the neutron background, and we find consistency within the statistical errors. This also indicates that no sizable neutron background was present.

*Hydrogen/deuterium target.* The target consisted of three identical cylindrical vessels 10 cm in diameter and 91.4 cm long. They were mounted so that they could be moved transverse to the beam direction, and any one of the three could be centered on the beam line to an accuracy of  $\pm 0.15$  cm. During the experiment, one chamber was filled with hydrogen, one with deuterium, and the third was evacuated. This design eliminated the need for emptying and refilling targets with deuterium or hydrogen, thus avoiding transients in density associated with filling. The vapor pressure above both the hydrogen and deuterium was measured to

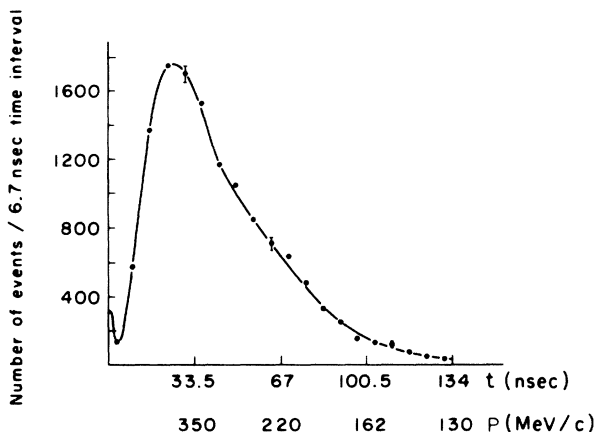


FIG. 2. Time-of-flight spectrum of the detected events observed at the position of our kaon detector. The small peak near zero time is due to the  $\gamma$ -ray contamination in the sample. The momentum scale corresponds to particles of the mass of  $K_L^0$  meson.

an accuracy of  $\pm 0.001$  atm, which allowed fluctuations of  $\sim 10^{-4}$  in the density to be observed. The lengths of the cylinders were measured during operation to an accuracy of  $\pm 0.08$  cm using telescopes and viewing ports at the ends of the targets. The effective length of the target is not exactly the measured over-all length, due to the curvature of the end domes. The correction for this effect, amounting to a length reduction of 0.6 cm, was calculated assuming the beam was uniformly distributed over the area given by the exit aperture of the primary collimator.

*Kaon detector.* The detector, described in detail in II, was designed on the principle that nearly all charged particles emerging from the evacuated neutral beam arise from kaon decay. It consisted of four two-counter telescopes, each 1.22 m in length but of different width, placed parallel to the beam line. They formed the sides of an open-ended asymmetrical box through whose open ends the beam passed. The sides of the box were made of unequal size in order to increase our sensitivity to possible backgrounds, since the five possible ratios of the rates in the six different telescope combinations are calculable for events arising from kaon decay. (For a symmetric detector, four of these ratios are equal due to symmetry alone.) The counters of each telescope were separated by a 0.64-cm thick steel plate to reduce neutron backgrounds. The geometrical efficiency of the detector was calculated to be 19% for 300 MeV/ $c$  kaons decaying into charged secondaries in the decay region, which extended from 60 cm upstream of the detector to its downstream edge. Beyond each telescope was placed shielding which was thick enough to stop all kaon decay products.

A large scintillation counter which served as a cosmic-ray veto was placed on the outside of each side of the detector, and a veto counter with a hole for the beam covered the upstream end of the detector.

*Monitors.* The principal beam monitor, which we call "S", was a telescope consisting of three  $1.3 \times 1.3 \times 0.6$  cm<sup>3</sup> scintillation counters spaced 30 cm apart. It was placed in a 750-MeV/c negative beam which was produced from the synchrotron target at an angle of 20°. Over time periods comparable to the target cycling time, random variations of approximately  $\pm 2\%$  were observed in the ratio of the rate of this monitor to the rate of detected kaons. The cause of these fluctuations is unknown, but correlations between these fluctuations and other measured quantities have been found. These correlations have been used to correct the monitor reading to some extent. However, the fluctuations in the corrected monitor still give rise to a normalization uncertainty of  $\pm 1.0$  mb for the double-chopped data and  $\pm 1.4$  mb for the single chopped data. Accidental counts in the monitor amounted to only about  $7 \times 10^{-4}$  of the rate. In addition to its use as a beam intensity monitor, S was used as a timing signal in the calibration of the time-of-flight system.

The secondary monitors we used were BOT (beam-on-target monitor, described in I) and G, a telescope consisting of three small scintillation counters, which was placed directly in the neutral beam upstream of the primary collimator. They provided cross checks on the normalization and helped to correct for some of the fluctuations observed in S.

A 156.25-kHz clock was used to monitor the live time of the experiment. This was needed for the calculation of the cosmic-ray background. In order to keep the cosmic-ray trigger rate to a minimum, we gated the experiment off when the synchrotron beam intensity was low. Thus the live time for the experiment changed significantly with the performance of the synchrotron.

To reduce our sensitivity to the variation of the proton beam energy during the spill, the four monitors were routed to different scalers in four different time periods of the spill. The characteristics of the beam in the four time periods are discussed in II. Only data from the fourth time period, where the proton energy reached its peak, were used for the evaluation of the cross sections.

*Time-of-flight system.* The time-of-flight system used to measure the  $K_L^0$  momentum is described in II. The time measurement was performed by starting a time to amplitude converter (TAC) with a timing signal and stopping it with an "event" pulse. This pulse, which signaled the arrival of a

kaon, was a coincidence between at least two of the four telescope combinations. The timing of the leading edge of the event pulse was determined by the telescope pulse which arrived latest. Since the phototubes were placed on the downstream ends of all of the counters, the decay particle which entered a telescope furthest upstream determined the timing of the event pulse.

The timing signal for the "start" input to the TAC was obtained from a counter located near the synchrotron target rather than from the synchrotron rf pulse as was done in I. This avoided the changes in relative phase between the targeting and the rf pulse during the beam spill. The timing counter, called  $T_0$ , was a water-filled Čerenkov counter located approximately 60 cm from the synchrotron target. The calibration of the TOF system used the rf frequency of PPA, calibrated delay cables, and the flight time of  $\gamma$  rays from the synchrotron target to the detector as primary standards.

*Data acquisition system.* The equipment used for the handling and storage of data was identical to that used in II. For each event the following information was recorded: (1) the counters which responded, (2) the TOF information, and (3) the number of the spill correlator channel in which the event occurred. Every twelfth event, the scalers containing monitoring data were read and recorded on magnetic tape.

A PDP-9 computer was used for transferring the information from the scalers and counter latches onto magnetic tape. It was also used to check for consistency of the various monitor ratios and to display the time-of-flight spectrum and histograms on a computer-controlled oscilloscope. This feedback was useful for checking the over-all operation of the experiment and for performing the timing calibrations.

An unavoidable background came from cosmic rays which made coincidences in two of the counter telescopes. The cosmic-ray anticoincidence shield surrounded most of the detector, but inefficiency at the level of 0.2% still allowed a background which amounted to about 1% of the real event rate. The cosmic-ray background was monitored continuously by recording events which appeared to be genuine but occurred during the time outside the beam spill. Since the same information was recorded for these events as for normal events, it was possible to evaluate the cosmic-ray background for each type of telescope coincidence pattern separately.

## B. Operating procedure

A complete set of data consisted of a measurement of the kaon rate with the vacuum target, the

deuterium target, and the hydrogen target. Each set of data took about eight hours to complete, and beam time was divided as follows: vacuum, 37%; hydrogen, 43%; and deuterium, 20%. By changing the target in the beam several times each day, the importance of experimental conditions which varied slowly with time, such as drifts in the monitors and kaon detector efficiency, was reduced.

Approximately once each day, the TOF system was calibrated by recording TOF data on  $\gamma$  rays in the beam. This was done by placing a thin lead converter upstream of the third magnet and deflecting the electron-positron pairs into the detector counters using that magnet. The time scale of the system was established by observing the spacing between successive peaks, which was equal to the known synchrotron rf period. The kaon TOF was measured relative to the  $\gamma$ -ray TOF, so the zero offset for the system was also established by this method.

The vapor pressure and target length for both hydrogen and deuterium targets were recorded once per day. The mean values of these quantities and their long-term fluctuations are displayed in Table I. Although it is possible to correct the data for observed fluctuations in both target length and vapor pressure, we have not done so, since the error introduced through treating them as constants is small compared to the over-all normalization uncertainty.

Part of the running period was devoted to collecting data with the mercury plug in the primary collimator filled, in order to determine the fraction of background events due to particles produced by the synchrotron which did not follow the beam line. The rate observed with the plug closed was slightly higher than the rate expected from cosmic ray events alone. The measured machine-induced plug closed background is  $(0.17 \pm 0.07)\%$  of the normal event rate, which is small enough to be ignored.

A run was also made in which the beam line was maintained at atmospheric pressure to check for the effect of neutron interactions in the beam line. A  $(5 \pm 1)\%$  increase in the event rate was observed. Since the beam line pressure was always less

than  $10 \mu$  during the normal runs, the background from this effect is negligible.

### C. Data reduction

The information stored on magnetic tape for each event was used to calculate the momentum and to separate events according to target, telescope combination, and correlator channel. The scalar data which were recorded on the same tape allowed us to obtain the number of monitor counts and evaluate the cosmic-ray background for a given set of data. The number of events in each bin was normalized to the corresponding number of  $S$  monitor counts, and a "raw" cross section was calculated as a function of momentum. Corrections for backgrounds, as well as corrections for systematic effects in the TOF measurement, were made to these cross sections.

*Momentum determination.* For each event, the kaon time of flight was determined from the output pulse height from the TAC, using two calibration constants, the TOF for  $\gamma$  rays,  $t_\gamma$ , and the conversion factor between time and pulse height. The momentum resolution is a complicated function based on several uncertainties in the TOF system. The effects which dominated the uncertainties were (1) the width of the proton bunch striking the production target, (2) the length of the kaon detector along the beam, and (3) the difference in the detector irradiation patterns for kaon decay products and for electron-positron pairs used to determine  $t_\gamma$ . Below 320 MeV/c the momentum resolution is fairly constant between 1% and 1.5% FWHM. Above 320 MeV/c it rises fairly rapidly to about 6% at 550 MeV/c. The principal effect is a smearing of the spectrum, and therefore little error is introduced into the evaluation of cross section versus momentum. The position of the effective center of the detector needed for the determination of the value of  $t_\gamma$  was determined by studying the shape of the  $\gamma$ -ray TOF spectrum. We estimate that the uncertainty in this position introduces an over-all 2% uncertainty in the momentum scale factor.

*Evaluation of the cross sections.* At a distance

TABLE I. Target data. Uncertainties shown are due to long-term fluctuations.

Target	Vapor pressure (psia)	Nuclear density $\rho$ (cm) <sup>-3</sup>	Effective target length $l$ (cm)	$1/\rho l$ (mb)
H <sub>2</sub>	15.25 ± 0.04	$(0.4220 \pm 0.0001) \times 10^{23}$	90.70 ± 0.10	261.3 ± 0.3
D <sub>2</sub>	5.59 ± 0.04	$(0.5068 \pm 0.0002) \times 10^{23}$	90.73 ± 0.10	217.5 ± 0.3

$L$  from the synchrotron target, the number of kaons of momentum  $P$  detected by our apparatus with a hydrogen target in the beam is given by

$$n_H(P) = M_H \left[ N_0(P) \epsilon(P) e^{-(m_K L / P \tau)} e^{-[\sigma_w(P) \rho_w l_w]} \right] \times e^{-[\sigma_H(P) \rho_H l_H]}, \quad (1)$$

in which  $M_H$  is the number of counts in the beam monitor,  $N_0(P)$  is the number of  $K_L^0$  produced at the synchrotron target per beam monitor count,  $\epsilon(P)$  is the detection efficiency of the apparatus,  $\tau$  is the  $K_L^0$  mean life and  $\sigma_H$ ,  $\rho_H$ , and  $l_H$  ( $\sigma_w$ ,  $\rho_w$ , and  $l_w$ ) are the total cross section, number density, and length of the hydrogen (target walls,) respectively. When the empty target is placed in the beam line, the number of detected events  $n_V(P)$  is the quantity in brackets in Eq. (1) multiplied by the number of monitor counts  $M_V$ . Therefore, in the absence of any background counts, the hydrogen total cross section is given by

$$\sigma_H(P) = \frac{1}{\rho_H l_H} \ln \left( \frac{n_V(P) M_H}{n_H(P) M_V} \right).$$

The values of  $1/\rho l$  for our targets are shown in Table I, and raw cross section calculated according to this formula and from the corresponding formula for deuterium are given in the second columns of Tables II–V.

*Corrections to the cross sections.* All data were corrected for cosmic-ray backgrounds. The ghost subtraction (discussed below) was negligible for the data taken with double-chopped injection. The two sets of data were corrected separately and the corrected data were combined to give the final results. Tables II–V list the corrections. Except for the TOF zero shift correction (discussed below), the raw data were corrected and the cross sections were recalculated using the corrected data. For those corrections, the differences between the corrected and uncorrected cross sections are listed and serve only to indicate the magnitude of the effects involved.

*Cosmic-ray correction.* Spurious events arise from cosmic rays which simulate a kaon decay by entering the apparatus without tripping a veto counter. Only events which occur soon after a proton bunch strikes the synchrotron target are registered, since only these events will be associated with a  $T_0$  pulse giving a valid TOF measurement. We monitor (a) the detection rate for cosmic rays and (b) the TOF efficiency, defined as the probability that a random event (like a cosmic-ray event) would have a valid TOF. Measurement (a) was made by recording the detector triggers during a period when the proton beam was not striking the target. Measurement (b) was made during the

beam spill by measuring random coincidences between a pulser signal and the  $T_0$  signal in the same manner as in the TOF system. The total cosmic-ray background was then computed from measurements (a) and (b), using also the measured live time for the detector. The cosmic-ray background correction is significant only at the lowest momenta where the relative kaon intensity was low.

*Ghost correction.* Because the flight times are measured modulo  $T_p$ , the proton bunch spacing, events for which the flight time is greater than  $t_\gamma + T_p$  are assigned an incorrect time of flight. These events are referred to as “ghosts.” We took approximately 80% of our data with single-chopped injection ( $T_p \approx 67$  ns) and the remaining 20% with double-chopped injection ( $T_p \approx 134$  ns). As can be seen by observing the spectrum taken with double-chopped injection (Fig. 2), the ghost contamination for flight times greater than 134 ns is negligible, but substantial corrections must be made for the single-chopped data. The contribution of the ghosts to the spectrum taken with the empty target  $G_V(t)$  is measured from the 134 ns spectrum. From this spectrum, the ghost contamination of the spectrum with the hydrogen target  $G_H(t)$  is calculated from

$$G_H(t) = G_V(t) \frac{M_H}{M_V} e^{-[\sigma_H(t + T_0) \rho_H l_H]}, \quad (2)$$

in which  $\sigma_H(t + T_p)$ , the cross section for kaons whose TOF is  $t + T_p$ , is determined from the data taken with double-chopped injection. The ghost spectrum for the deuterium data is obtained in a similar way. The ghost subtraction was important for high momenta which were contaminated by low-momentum kaons with larger cross sections. Due to the “folding over” of the time spectrum, some  $\gamma$ -ray background events appeared in the lowest-momentum bin. They were also removed by this subtraction, but the correction is in error, because in Eq. (2) we assumed that the ghosts are kaons. Because of this uncertainty in the subtraction of  $\gamma$ -ray events, we have not included the lowest-momentum point of the single-chopped data in our final data set.

*Timing correction* Toward the end of the running period, it was discovered that the train of  $T_0$  pulses derived from the timing counter was occasionally contaminated by spurious pulses, which resulted in a measured time-of-flight different from the correct one for a fraction (<10%) of the events.

Using the kaon momentum spectrum taken after the malfunction was corrected, it was possible to correct the much larger sample of data taken with

the spurious pulses present. It was possible to do this reliably since the distortion of the momentum spectrum was independent of the target. Except for the cross sections at very low momenta, corrections were small compared to the statistical uncertainty. The correction was significant at low momenta, since the effect of the timing error was to shift events of high momenta and small cross sections into the relatively unpopulated low-momentum part of the spectrum. Because the correction is important only at low momenta, it was applied only to the double-chopped data.

*TOF-zero-shift correction.* Since the measurement of the cross section in this experiment is made by comparing a TOF spectrum with the target empty to one with the target full, a shift in the zero of the TOF measurement will give rise to an error in the cross section. At a given momentum, the error introduced is proportional to the slope of the spectrum, and since the spectrum is not flat, the error is momentum-dependent. This effect has been treated previously by Devlin *et al.*<sup>3</sup> Although the TOF system was calibrated frequently, shifts in the zero were observed at the level of  $\pm 0.15$  ns. Since the effect of the zero shift is simply related to the cross section through the shape of the momentum spectrum, it is a simple matter to propagate this uncertainty to an uncertainty in the cross sections. However, at the higher momenta, the uncertainties are very large,

and this method also introduces correlations between the measurements at different momenta. We have therefore chosen to use the total cross-section data of charged kaons on hydrogen and deuterium which overlap our data at the higher momenta to calculate the effective zero shift for our data and to simply apply a correction for this effect. We assume charge independence to calculate the  $K_L^0p$  and  $K_L^0d$  cross sections from the data of Bowen *et al.*<sup>4</sup> in the momentum range 366–536 MeV/c. We then calculate the value of the TOF-zero shift which best adjusts our data in that momentum range to give agreement with the cross sections derived from the charged kaon data. The values obtained for the zero shifts are given in Tables II–V, and they all lie within the observed uncertainty in our measurement of the actual zero shift. The corrected data are in satisfactory agreement with the data of Bowen *et al.*, whereas some of the data sets showed poor agreement before the corrections were made. As can be seen in Tables II–V, the corrections are largest for the higher momentum points, and it is only for that portion of the data that the correction becomes larger than the statistical errors.

*Miscellaneous corrections.* Other corrections which have been investigated but found to be negligible are (1) forward scattering correction ( $<0.02\%$ ); (2) inefficiency in the injection chopper, measured to be typically  $0.1\%$ , which would

TABLE II.  $K_L^0p$  total cross sections obtained with single-chopped injection.

$p^a$ (MeV/c)	$\sigma_p$ (raw) (mb)	Ghost correction (mb)	Cosmic-ray correction (mb)	TOF- zero-shift correction <sup>b</sup> (mb)	$\sigma_p$ (corrected) <sup>c</sup> (mb)
210–230	44.2±4.2	-1.7	-0.4	1.0	43.0±5.0
230–250	45.7±2.7	-1.0	-0.1	0.0	44.5±3.0
250–270	36.5±2.6	-1.7	-0.2	0.0	34.6±2.9
270–290	38.1±2.7	-1.8	-0.1	-0.2	36.0±3.0
290–310	29.9±2.7	-2.6	-0.1	-0.6	26.6±3.0
310–330	34.8±2.7	-2.4	-0.1	-0.8	31.4±3.1
330–350	27.3±2.8	-3.3	-0.1	-1.0	22.8±3.2
350–370	28.0±2.9	-3.4	-0.1	-1.2	23.2±3.3
370–390	22.5±3.0	-4.2	-0.1	-2.0	16.1±3.5
390–410	25.6±3.2	-4.1	-0.1	-2.6	18.8±3.7
410–430	28.2±3.4	-4.1	-0.1	-3.6	20.4±4.0
430–450	24.2±3.6	-4.9	-0.1	-4.8	14.2±4.4
450–470	27.3±3.8	-4.8	-0.1	-6.0	16.3±4.7
470–490	25.6±4.1	-5.5	-0.1	-7.2	12.7±5.2
490–510	26.6±4.3	-5.8	-0.2	-8.9	11.8±5.7
510–530	29.9±4.7	-5.7	-0.2	-10.7	13.4±6.4
530–550	28.5±5.0	-6.5	-0.2	-12.5	9.3±7.2

<sup>a</sup>Momentum scale factor is  $1.00 \pm 0.2$ .

<sup>b</sup>Fitted value of relative TOF-zero shift is  $(0.20 \pm 0.05)$  ns.

<sup>c</sup>The absolute normalization uncertainty is  $\pm 1.4$  mb.

TABLE III.  $K_{\mathcal{D}}^0 p$  total cross sections obtained with double-chopped injection.

$P^a$ (MeV/c)	$\sigma_p$ (raw) (mb)	Timing correction (mb)	Cosmic-ray correction (mb)	TOF- zero-shift correction <sup>b</sup> (mb)	$\sigma_p$ (corrected) <sup>c</sup> (mb)
130–150	46.1±6.6	12.9	2.7	4.5	66.2±13.5
150–170	53.7±5.9	10.6	1.4	3.4	69.0±9.1
170–190	53.5±5.1	3.8	0.5	2.2	60.0±6.2
190–210	43.3±4.7	0.6	0.2	1.5	45.6±4.9
210–230	48.4±4.5	0.3	0.2	0.9	49.7±4.6
230–250	21.2±4.4	0.3	0.0	0.0	21.5±4.3
250–270	27.5±4.5	0.1	0.0	0.0	27.6±4.3
270–290	41.7±4.5	-0.1	0.1	-0.2	41.4±4.4
290–310	27.9±4.6	0.1	0.0	-0.6	27.4±4.4
310–330	27.1±4.7	0.3	0.0	-0.7	26.6±4.4
330–350	27.1±4.8	0.2	0.0	-0.9	26.4±4.6
350–370	27.0±5.0	0.3	0.0	-1.1	26.1±4.6
370–390	25.0±5.2	0.4	0.0	-1.9	23.6±5.0
390–410	23.1±5.5	0.7	0.0	-2.4	21.4±5.0
410–430	10.7±5.9	1.9	0.0	-3.3	9.2±5.5
430–450	15.8±6.3	1.9	0.0	-4.5	13.1±5.8
450–470	33.0±6.7	-0.2	0.0	-5.6	27.2±6.3
470–490	20.2±7.1	0.8	0.0	-6.7	14.2±7.1
490–510	8.4±7.8	2.7	0.0	-8.2	2.8±7.5
510–530	23.0±8.3	0.3	0.0	-9.9	13.4±8.8
530–550	21.5±9.1	-0.1	0.0	-11.6	9.9±10.0

<sup>a</sup>Momentum scale factor is  $1.00 \pm 0.02$ .<sup>b</sup>Fitted value of relative TOF-zero shift is  $(0.19 \pm 0.07)$  ns.<sup>c</sup>Absolute normalization uncertainty is  $\pm 1.0$  mb.TABLE IV.  $K_{\mathcal{D}}^0 d$  total cross sections obtained with single-chopped injection.

$P^a$ (MeV/c)	$\sigma_D$ (raw) (mb)	Ghost correction (mb)	Cosmic-ray correction (mb)	TOF- zero-shift correction <sup>b</sup> (mb)	$\sigma_D$ (corrected) <sup>c</sup> (mb)
210–230	94.3±4.2	-3.9	1.0	0.4	91.7±4.7
230–250	90.6±2.6	-2.7	0.3	0.0	88.2±2.8
250–270	86.8±2.6	-3.4	0.2	0.0	83.7±2.9
270–290	82.8±2.6	-3.8	0.2	-0.1	79.1±2.9
290–310	78.6±2.6	-4.2	0.2	-0.2	74.3±2.9
310–330	71.2±2.7	-4.9	0.1	-0.3	66.0±3.0
330–350	69.2±2.8	-5.3	0.1	-0.4	63.5±3.1
350–370	71.3±2.9	-5.4	0.1	-0.4	65.6±3.2
370–390	64.0±3.0	-6.2	0.1	-0.7	57.1±3.4
390–410	64.2±3.1	-6.4	0.1	-0.9	56.9±3.5
410–430	65.9±3.3	-6.7	0.1	-1.3	57.9±3.8
430–450	59.1±3.5	-7.8	0.1	-1.7	49.5±4.1
450–470	62.5±3.7	-7.9	0.0	-2.8	52.4±4.5
470–490	57.8±3.9	-9.1	0.0	-2.6	46.1±4.8
490–510	61.9±4.2	-9.3	0.0	-3.2	49.5±5.3
510–530	64.0±4.6	-10.1	0.0	-3.8	50.0±6.0
530–550	64.5±4.9	-11.2	0.0	-4.5	48.8±6.6

<sup>a</sup>Momentum scale factor is  $1.00 \pm 0.02$ .<sup>b</sup>Fitted value of relative TOF-zero shift is  $(0.09 \pm 0.05)$  ns.<sup>c</sup>The absolute normalization uncertainty is  $\pm 1.4$  mb.

TABLE V.  $K_L^0 d$  total cross sections obtained with double-chopped injection.

$P^a$ (MeV/c)	$\sigma_D$ (raw) (mb)	Timing correction (mb)	Cosmic-ray correction (mb)	TOF- zero-shift correction <sup>b</sup> (mb)	$\sigma_D$ (corrected) <sup>c</sup> (mb)
130-150	102.3 ± 6.9	29.5	11.3	1.1	144.1 ± 15.8
150-170	110.6 ± 6.1	20.0	4.9	0.8	136.3 ± 10.3
170-190	107.0 ± 5.4	6.4	1.9	0.5	115.8 ± 6.6
190-210	100.3 ± 4.8	1.5	0.9	0.4	103.1 ± 5.2
210-230	94.9 ± 4.6	0.4	0.6	0.2	96.1 ± 4.7
230-250	75.2 ± 4.5	-0.1	0.3	0.0	75.4 ± 4.4
250-270	73.8 ± 4.5	-0.1	0.3	0.0	74.0 ± 4.4
270-290	81.0 ± 4.5	-0.1	0.3	0.0	81.1 ± 4.5
290-310	69.9 ± 4.6	0.0	0.2	-0.1	70.0 ± 4.4
310-330	69.2 ± 4.7	0.1	0.2	-0.2	69.3 ± 4.4
330-350	65.6 ± 4.8	0.2	0.1	-0.2	65.7 ± 4.6
350-370	67.7 ± 5.0	0.2	0.1	-0.3	67.8 ± 4.7
370-390	58.9 ± 5.2	0.7	0.1	-0.4	59.3 ± 4.9
390-410	56.1 ± 5.4	1.4	0.1	-0.6	56.9 ± 5.0
410-430	44.6 ± 5.8	2.3	0.1	-0.8	46.2 ± 5.4
430-450	44.0 ± 6.2	3.2	0.1	-1.1	46.3 ± 5.6
450-470	52.0 ± 6.5	1.8	0.1	-1.3	52.6 ± 6.1
470-490	53.5 ± 7.1	1.3	0.1	-1.6	53.2 ± 6.9
490-510	44.8 ± 7.6	3.0	0.1	-2.0	45.9 ± 7.2
510-530	53.3 ± 8.2	0.7	0.1	-2.3	51.6 ± 8.5
530-550	56.1 ± 9.0	-0.1	0.1	-2.7	53.3 ± 9.7

<sup>a</sup>Momentum scale factor is  $1.00 \pm 0.02$ .<sup>b</sup>Fitted value of relative TOF zero shift is  $(0.05 \pm 0.07)$  ns.<sup>c</sup>Absolute normalization uncertainty is  $\pm 1.0$  mb.

produce effects similar to ghosts, but smaller by at least an order of magnitude; (3) uncertainty in the measurements of target length ( $< 0.3\%$ ) and density ( $< 0.2\%$ ). Quantities given are upper estimates of the fractional changes in the cross sections introduced by these effects.

*Final results.* The results of the corrections discussed above are summarized in Tables II-V, along with the final corrected cross sections. The results for hydrogen are in agreement with the data of Sayer *et al.*<sup>1</sup> obtained by a polyethylene-carbon subtraction. The results for single-chopped and double-chopped data are mutually consistent, with the exception of one data point. This apparent discrepancy is due to the two 230-250 MeV/c data points for hydrogen, which disagree by 4.4 standard deviations. This appears to be an improbable statistical fluctuation, since the two points appear to be fluctuations in opposite directions from a smooth curve drawn through the neighboring points. A similar but smaller effect is seen in deuterium, but correlations are expected, since the same vacuum data are used for both. With the exception of these two points, the sum of the squares of the residuals between the data sets are 8.8 for the 16 hydrogen data points and 14.0 for the 17 deuteri-

um data points.

A final data set was obtained by using the five lowest-momentum points from the double-chopped data and averaging the double-chopped and single-chopped data for the higher-momentum points. These final results are given in Table VI. We advise readers who wish to combine these results with other data to use the results listed in Tables II-V with their normalization errors rather than the results listed in Table VI. A different normalization for the double-chopped and single-chopped data would cause a systematic shift for the five double-chopped data points which were not averaged with the single-chopped data.

The uncertainties in absolute normalization arise from observed variations in the ratio of the S monitor rate to the rate of detected kaons. A graph of the ratio of detected kaons to the monitor rate is shown in Fig. 3. The rms fractional fluctuations  $\delta x$  in this ratio were found to be 0.010 for the double-chopped data and 0.016 for the single-chopped data. The corresponding normalization uncertainty is related to  $\delta x$  by  $\delta\sigma = 2\delta x/\rho l\sqrt{N}$ , in which  $N$  is the total number of runs. The resulting normalization uncertainties are given in Tables II-V. Because of the inadvisability in using the average

cross section for fitting purposes, we do not quote a normalization uncertainty for the average cross sections of Table VI. As mentioned above, the momentum scale factor has an uncertainty of  $\pm 2\%$ , due to our uncertainty in the effective center of our detector.

### III. INTERPRETATION OF THE DATA

#### A. $K_L^0 p$ total cross sections

The  $K_L^0 p$  total cross sections are of interest primarily for the  $\bar{K}N$  parameterization problem, since in the energy region of interest the  $KN$  amplitudes are much smaller than the  $\bar{K}N$  amplitude. The  $\bar{K}N$  amplitudes for the  $K_L p$  system are pure isospin 1, whereas both the  $I=0$  and  $I=1$   $KN$  amplitudes are present. In this energy region, the  $KN$  amplitudes are described with sufficient accuracy by a simple  $S$ -wave scattering length with a nonzero effective range for the isospin 1 amplitude. For the  $KN$  scattering lengths and effective ranges we have used<sup>5</sup>  $a_0=0.04$  F,  $a_1=-0.32$  F,  $r_0=0$ , and  $r_1=0.31$  F, where the subscript indicates the isospin state. The  $\bar{K}N$  amplitudes are much larger than the  $KN$  amplitudes, and due to the strong coupling between the three possible final-state channels, ( $\bar{K}N, \Sigma\pi, \Lambda\pi$ ), a  $K$ -matrix formalism<sup>6</sup> is used for their description. In recent years, a number of analyses<sup>7-10</sup>

TABLE VI. Final results for  $K_L^0 p$  and  $K_L^0 d$  total cross sections.

$P^a$ (MeV/c)	$\sigma_p^b$ (mb)	$\sigma_D^b$ (mb)
130-150	66.2 $\pm$ 13.5	144.1 $\pm$ 15.8
150-170	69.0 $\pm$ 9.1	136.3 $\pm$ 10.3
170-190	60.0 $\pm$ 6.2	115.8 $\pm$ 6.6
190-210	45.6 $\pm$ 4.9	103.1 $\pm$ 5.2
210-230	46.7 $\pm$ 3.4	93.9 $\pm$ 3.3
230-250	37.1 $\pm$ 2.5	84.4 $\pm$ 2.4
250-270	32.4 $\pm$ 2.4	80.7 $\pm$ 2.4
270-290	37.7 $\pm$ 2.5	79.7 $\pm$ 2.4
290-310	26.8 $\pm$ 2.5	73.0 $\pm$ 2.5
310-330	29.8 $\pm$ 2.5	67.1 $\pm$ 2.5
330-350	24.0 $\pm$ 2.6	64.3 $\pm$ 2.6
350-370	24.2 $\pm$ 2.7	66.3 $\pm$ 2.6
370-390	18.6 $\pm$ 2.9	57.8 $\pm$ 2.8
390-410	19.7 $\pm$ 2.9	56.9 $\pm$ 2.8
410-430	16.5 $\pm$ 3.2	54.0 $\pm$ 3.1
430-450	13.8 $\pm$ 3.5	48.4 $\pm$ 3.3
450-470	20.2 $\pm$ 3.8	52.5 $\pm$ 3.6
470-490	13.2 $\pm$ 4.2	48.5 $\pm$ 4.0
490-510	8.5 $\pm$ 4.5	48.2 $\pm$ 4.3
510-530	13.4 $\pm$ 5.2	50.6 $\pm$ 4.9
530-550	9.5 $\pm$ 5.8	50.4 $\pm$ 5.5

<sup>a</sup> Momentum scale factor is  $1.00 \pm 0.02$ .

<sup>b</sup> We advise against using the averaged cross sections from this table when combining our results with other data sets, and therefore we do not quote a normalization uncertainty. See text for the discussion of this point.

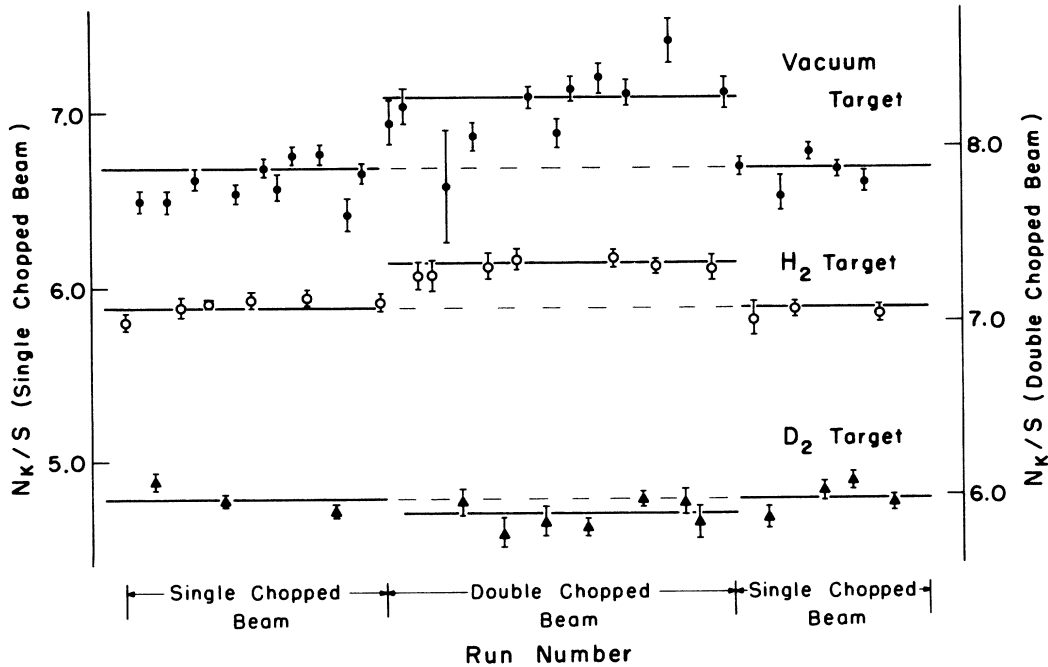


FIG. 3. Ratio of detected kaons to corrected  $S$ -monitor counts for 2-6 hour data-taking runs, showing the time sequence in which they were taken. The horizontal lines are the mean values used in obtaining the absolute values of the total cross sections. The scatter of these points about their mean is too large to be explained by statistical errors alone, and they give rise to an absolute normalization uncertainty in the total cross sections of  $\pm 1.0$  mb for the double-chopped data and  $\pm 1.4$  mb for the single-chopped data.

have been carried out, in which the existing  $\bar{K}N$  data in our energy interval have been parameterized in various ways. They differ in the number of partial waves included, the use of effective range parameters, and in the parameterization of the partial waves higher than  $s$  waves. The reader is referred to the original papers for details.

We have compared our data with these  $\bar{K}N$  parameterizations, leaving no constants adjustable except the over-all normalization constants, which were constrained by our estimated normalization uncertainty. Since the parameterizations are applicable at low energies, we have restricted our comparison to data points in this momentum range 130–450 MeV/ $c$ . We have used all our  $K_L^0 p$  data in this range except the two 230–250 MeV/ $c$  data points, which are internally inconsistent, as mentioned above. The calculated values of the cross sections are shown in Fig. 4, and the results of the comparisons are given in Table VII. As can be seen by examining the  $\chi^2$  values, our data are best fitted by the two parameterizations of Thompson, one<sup>8</sup> (T1) a constant  $K$ -matrix parameterization and the other<sup>10</sup> (T2) an energy-dependent  $K$ -matrix parameterization. The parameterization of Martin and Ross<sup>7</sup> shows fair agreement with our data, especially at the lower momenta, whereas the parameterization of Kim<sup>9</sup> fails rather badly to fit our data. This failure is not surprising, since the inability of the Kim parameters to fit the low-momentum  $\bar{K}N$  charge exchange data has already been pointed out.<sup>10</sup>

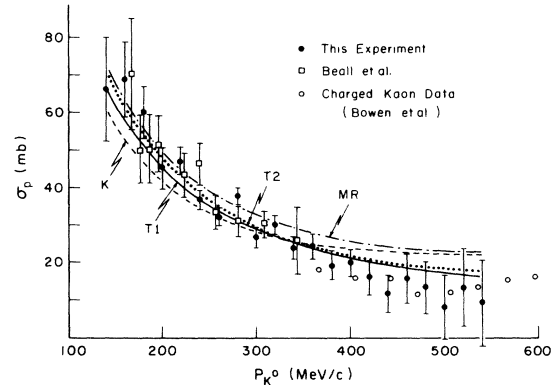


FIG. 4. Values of the  $K_L^0 p$  total cross sections averaged over the two data sets, shown with the four expected curves calculated from the results of the  $\bar{K}N$   $K$ -matrix fits. The curve labels correspond to fits as follows: “MR”—Martin and Ross (Ref. 7); “T1”—constant  $K$ -matrix fit of Thompson (Ref. 8); “K”—Kim (Ref. 9); “T2”—energy-dependent  $K$ -matrix fit of Thompson. See the footnotes to Table VII for more information on these analyses. For comparison, values of the  $K_L^0 p$  total cross sections calculated from the charged kaon total cross-section data of Bowen *et al.* (Ref. 4) are also shown.

#### B. $K_L^0 d$ total cross sections

A comparison of the  $K_L^0 d$  data with theoretical calculations is of interest primarily for the pur-

TABLE VII. Comparison of measured  $K_L^0 p$  total cross sections with existing  $K$ -matrix fits to other  $\bar{K}N$  data. As discussed in the text, we have used all our data below 450 MeV/ $c$  in these fits except the 230–250 MeV/ $c$  data points, which appear to be internally inconsistent between the double- and single-chopped data sets.

Analysis	Curve label	Single-chopped data (210–450) MeV/ $c$		Double-chopped data (130–450) MeV/ $c$		Both data sets $\chi^2$ (27 d.f.)
		$\chi^2$ (10 d.f.)	$\Delta$ (mb) <sup>a</sup>	$\chi^2$ (17 d.f.)	$\Delta$ (mb) <sup>a</sup>	
Martin and Ross <sup>b</sup>	MR	19.2	2.9	24.5	1.2	43.7
Thompson <sup>c</sup>	T1	11.6	0.2	20.5	-0.4	32.1
Kim <sup>d</sup>	K	20.0	0.5	31.9	-0.5	51.9
Thompson <sup>e</sup>	T2	10.6	0.6	17.7	0.0	28.3

<sup>a</sup> $\Delta$  is the fitted value of the normalization constant, constrained to zero by our estimated uncertainty.

<sup>b</sup>See Ref. 7. We use the  $s$ -wave constant  $K$ -matrix fit with  $p$  waves parameterized in the constant-scattering-length approximation.

<sup>c</sup>See Ref. 8.

<sup>d</sup>See Ref. 9.

<sup>e</sup>J. Thompson, private communication. This energy-dependent constant  $K$ -matrix fit uses the same parameters that are used in Ref. 10 except that the momentum range of the fit was extended to include data between 0 and 450 MeV/ $c$ .

pose of understanding the approximations needed to describe three-body scattering at low momenta. Despite the limited statistical accuracy of this set of data, the  $K_L^0 d$  system has distinct advantages over other systems used for this purpose. The scattering of a charged particle from deuterium at very low-momenta results in both experimental and theoretical difficulties due to Coulomb forces, whereas the analysis of neutron-deuterium scattering encounters difficulties due to the Pauli principle.

Theoretical calculations for the  $K^- d$  scattering cross sections using different approximations have appeared in the literature<sup>11-13</sup> over the past several years. These calculations are somewhat obsolete since they have been made with crude parameterizations of  $\bar{K}N$  amplitudes which are inadequate to describe the presently available data; however, we feel that a comparison of the various calculational techniques is useful. We compare the theoretical values of the cross-section defect with the experimental one, defined by

$$\delta(K_L^0 d) = \sigma_{\text{tot}}(K_L^0 d) - \sigma_{\text{tot}}(K_L^0 p) - \sigma_{\text{tot}}(K_L^0 n),$$

in which  $\sigma_{\text{tot}}(K_L^0 d)$  is the experimentally measured cross section, and  $\sigma_{\text{tot}}(K_L^0 p)$  and  $\sigma_{\text{tot}}(K_L^0 n)$  are calculated quantities. For these, we use one of the parameterizations which adequately fit our  $K_L p$  total cross sections (the constant  $K$ -matrix fit of Thompson<sup>8</sup>) for the  $\bar{K}N$  amplitudes, and the  $s$ -wave effective range approximation<sup>5</sup> for the  $KN$  amplitudes. The values of the experimental cross-section defect obtained in this way are shown in Fig. 5.

Theoretical values of the cross-section defect for the  $K^- d$  system have been obtained by evaluating the theoretical values of the  $K^- p$  and  $K^- n$  total cross sections from the same parameters for the  $\bar{K}N$  amplitudes as was used in obtaining the theoretical  $K^- d$  total cross sections. Where calculations using more than one parameterization of the  $K^- d$  amplitudes have been reported, we choose that parameterization which most closely reproduces the  $K^- p$  and  $K^- n$  cross sections given by the constant  $K$ -matrix method. For this reason, we have used the calculations by Chand<sup>13</sup> made with the HRI solutions. We have chosen for comparison with our data the calculation of Hetherington and Schick<sup>11</sup> in which the mass-difference parameter is zero and the range parameter  $\beta^{-1}$  is 0.1 F.

Assuming charge independence, the relationship between the cross-section defect for  $K_L^0 d$  scattering and  $K^+ d$  scattering is simply

$$\delta(K_L^0 d) = \frac{1}{2} [\delta(K^- d) + \delta(K^+ d)].$$

Since the value of the  $K^+ d$  cross-section defect is only a few percent of the  $K^- d$  defect, we have ignored it in this comparison. We show in Fig. 5 the values of  $\delta(K^- d)/2$  obtained for each of the theoretical calculations. It appears that our data are well fitted by the three-body calculation of Hetherington and Schick<sup>11</sup> and the static model of Chand,<sup>13</sup> but that the multiple scattering calculation of Queen<sup>12</sup> gives values of the defect which are too large. It is reasonable that the approximation used by Chand, in which the recoil of the nucleons is ignored, fits total cross-section data well, since there is no recoil for elastic scattering in the forward direction.

Our method of obtaining the theoretical cross-sections defect is somewhat crude, and it is clear that it does not do justice to the calculations. The proper comparison could be made, however, if the calculations could be repeated using values of the  $\bar{K}N$  amplitudes obtained from one of the  $K$ -matrix methods.

Although Glauber theory<sup>14</sup> is normally considered a high-energy correction, we have evaluated the Glauber formula for the cross-section defect, given by

$$\delta_G(K_L^0 d) = \langle r_D^{-2} \rangle \sigma(K_L^0 p) \sigma(K_L^0 n) / 4\pi,$$

in which, following Armenteros *et al.*,<sup>15</sup> we have used for  $\langle r_D^{-2} \rangle$  the value  $0.0423 \text{ mb}^{-1}$ . We show in Fig. 5 the results of this calculation and remark only that it seems to fit our data as well as the

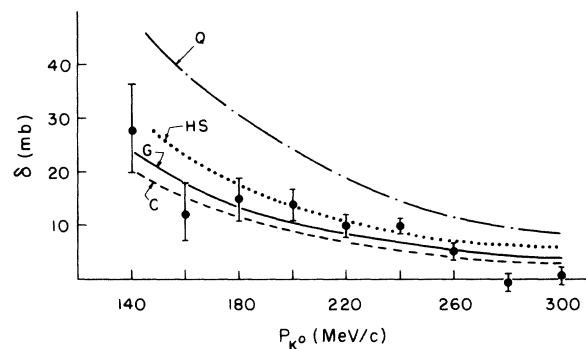


FIG. 5. Values of the  $K_L^0 d$  total cross section defect, defined as  $\delta = \sigma(K_L^0 d) - \sigma(K_L^0 p) - \sigma(K_L^0 n)$ . Theoretical values of this defect have been obtained from the calculations for  $K^- d$  scattering cross sections of Hetherington and Schick (HS) (Ref. 11), Queen (Q) (Ref. 12), and Chand (C) (Ref. 13), as discussed in the text. The curve marked G is an evaluation of the Glauber formula (Ref. 14).

more detailed calculations. We have not averaged the cross sections over the Fermi momenta of the nucleons in evaluating this formula.

Our final results for the  $K_L^0 d$  total cross sections, averaged over both data sets, are shown in Fig. 6. For comparison, we show the value calculated with the constant  $K$ -matrix fit of Thompson,<sup>8</sup> corrected with the Glauber formula.

#### ACKNOWLEDGMENTS

We are indebted to Professor M. G. White, Professor W. Wales, and the staff of the Princeton-Pennsylvania Accelerator for their excellent support during all stages of this work. Carl Meuhleisen provided technical assistance. One of (W.E.C.) would like to thank Dr. R. Landau and Dr. J. Thompson for helpful discussions.

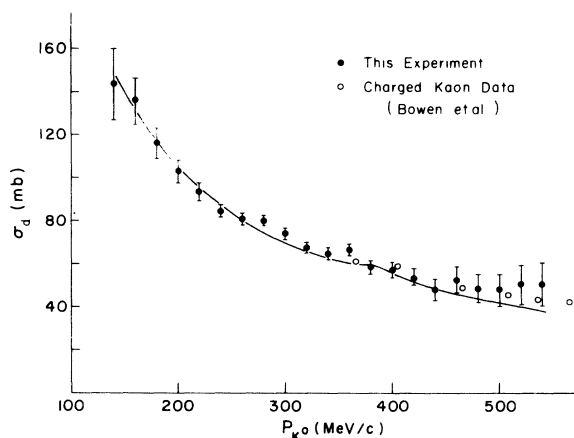


FIG. 6. Values of the  $K_L^0 d$  total cross sections averaged over the two data sets. The solid curve is the value calculated from the constant  $K$ -matrix fit of Thompson (Ref. 8), corrected with the Glauber formula. The open points are the averaged values of the  $K^+ d$  and  $K^- d$  total cross sections as measured by Bowen *et al.* (Ref. 4).

\*Work supported in part by National Science Foundation Grants Nos. GU-1592 and GP-14703 and USAEC Contract No. AT(30-1)-3651.

†Present address: Physics Department, University of Pittsburgh, Pittsburgh, Penn. 15260.

‡Present address: Stanford Linear Accelerator Laboratory, Stanford, Calif. 94305.

§Present address: 12 Topaz Court, Spring Valley, N.Y. 10977.

|| Present address: Philco-Ford, 3900 Welsh Road, Willow Grove, Penn. 19090.

¶ Present address: General Electric Research and Development Center, P. O. Box 8, Schenectady, N. Y. 12301.

<sup>1</sup>G. A. Sayer, E. F. Beall, T. J. Devlin, P. Shepard, and J. Solomon, *Phys. Rev.* **169**, 1045 (1968).

<sup>2</sup>Kirby G. Vosburgh, Thomas J. Devlin, Robert J. Esterling, Barton Goz, Douglas A. Bryman, and W. E. Cleland, *Phys. Rev. D* **6**, 1834 (1972).

<sup>3</sup>T. J. Devlin, W. Johnson, J. Norem, K. Vosburgh, R. E. Mischke, and W. Schimmerling, *Phys. Rev. D* **8**, 136 (1973).

<sup>4</sup>T. Bowen, P. K. Caldwell, F. Ned Dikmen, E. U. Jenkins, R. M. Kalbach, D. V. Petersen, and A. E. Pifer, *Phys. Rev. D* **2**, 2599 (1970).

<sup>5</sup>V. J. Stenger, W. E. Slater, D. H. Stork, H. K. Ticho,

G. Goldhaber, and S. Goldhaber, *Phys. Rev.* **134**, B1111 (1964); A. D. Martin and R. Perrin, *Nucl. Phys.* **B10**, 125 (1969).

<sup>6</sup>R. H. Dalitz and S. F. Tuan, *Ann. Phys. (N.Y.)* **10**, 307 (1960); Marc H. Ross and Gordon L. Shaw, *ibid.* **13**, 147 (1961).

<sup>7</sup>A. D. Martin and G. G. Ross, *Nucl. Phys.* **B16**, 479 (1970).

<sup>8</sup>J. Thompson, *Hyperon Resonances—70*, edited by Earle C. Fowler (Moore, Durham, North Carolina, 1970), p. 61.

<sup>9</sup>J. Kwan Kim, *Phys. Rev. Lett.* **19**, 1074 (1967).

<sup>10</sup>D. Berley, S. P. Yamin, R. R. Kofler, A. Mann, G. W. Meisner, S. S. Yamamoto, J. Thompson, and W. Willis, *Phys. Rev. D* **1**, 1996 (1970); J. Thompson (private communication).

<sup>11</sup>J. H. Hetherington and L. H. Schick, *Phys. Rev.* **141**, 1314 (1966).

<sup>12</sup>N. M. Queen, *Nucl. Phys.* **66**, 673 (1965).

<sup>13</sup>Ramesh Chand, *Ann. Phys. (N.Y.)* **22**, 438 (1963).

<sup>14</sup>R. J. Glauber, *Phys. Rev.* **100**, 242 (1955).

<sup>15</sup>A. Armenteros, P. Baillon, P. Lexa, A. Minten, K. H. Nguyen, E. Pagiola, V. Pelosi, R. Barloutaud, F. Bigitu, M. Crozon, C. Louedec, J. L. Narjoux, and F. Pierre, *Nucl. Phys.* **B18**, 425 (1970).